

# Measuring Properties of a CCD Spectrograph

1<sup>st</sup> Kryštof Havránek

Course: Space Engineering 2025

Czech Technical University in Prague

Technická 2, Prague, Czech Republic

havrakry@fel.cvut.cz

2<sup>nd</sup> Vega Grau Esteve

Course: Space Engineering 2025

Politecnical University of Valencia

Camino de Vera 46022, Valencia, Spain

vega03upv@gmail.com

Mentor

Course: Space Engineering 2025

Astronomical Institute of the CAS

Fričova 298, Ondřejov, Czech Republic

martin.jelinek@asu.cas.cz

**Abstract**—Following paper concerns itself with a process of measuring and calculating parameters of a Cloude CCD spectrograph connected to a Perek 2 meter optical telescope. Measured properties were readout noise, dark current behavior and lastly gain.

## I. INTRODUCTION

One of the primary tools used to investigate the physical properties of celestial objects is astronomical spectroscopy. This carries out a process that enables the determination of stellar temperatures, chemical composition, radial velocities and other fundamental parameters by dispersing incoming light into its constituent wavelengths. Nowadays, modern spectroscopic observations rely on large-aperture telescopes which are combined with sensitive CCD detectors and stable spectrographs.

As emphasized by Martinez et al. in A Practical Guide to CCD Astronomy, the scientific quality of CCD-based observations depends not only on the optical system but also on a precise understanding of detector behavior and noise sources, as well as on proper calibration procedures [1]. Similarly, Lessons from the Masters highlights that accurate spectroscopic measurements require careful instrument characterization and calibration before any scientific interpretation can be performed [2].

This protocol describes the instrumental setup and theoretical background relevant to spectroscopic observations carried out with the Ondřejov 2-m telescope. Particular emphasis is placed on the principles of spectrograph operation, CCD detector characteristics, and the main noise sources affecting the acquired data. This theoretical foundation provides the basis for the data reduction and analysis steps described in later sections.

## II. PEREK 2 M TELESCOPE

The Perek 2 m telescope (see 1), operated by the Astronomical Institute of the Czech Academy of Sciences, is built as a classical Coudé reflector with a 2 m primary mirror. The telescope provides a combination of high light-gathering power and mechanical stability, making it well suited for high-resolution spectroscopic observations of relatively faint astronomical targets [3].

In Coudé configuration incoming light is reflected from the primary mirror onto the secondary which then reflects it with flat mirrors into a coudé focus 2. From the telescope three

optical fibres bring the light to two different spectrographs – an echelle spectrograph and a single order spectrograph with focal length of 700 mm (referred to as coude spectrograph), on which this paper is focused.

This telescope is equipped with accurate guiding and tracking systems, which are essential for spectroscopic observations performed with narrow entrance slits or optical fibers. The systems implemented in the Ondřejov 2-m telescope ensure stable target positioning during long exposures. Guiding errors can directly lead to reduced signal-to-noise ratio or artificial broadening of spectral features, directly affecting the quality of the recorded spectra [2].



Fig. 1. Perek 2 m Telescope

## III. SPECTRAL ORDERS AND WAVELENGTH CALIBRATION

Spectrograph is an optical instrument designed in a way that incoming light is dispersed into its different wavelength components. In the field of scientific spectrographs, this kind of dispersion is achieved by using a diffraction grating. Grating is a prism with hundreds of grooves that act in a similar manner to a two slit experiment – it exploits constructive interference creating a maxima and minima for each wavelength. A different wavelength get reflected with different angles where following equation must be satisfied.

$$d \sin \theta_m = m\lambda, \quad (1)$$

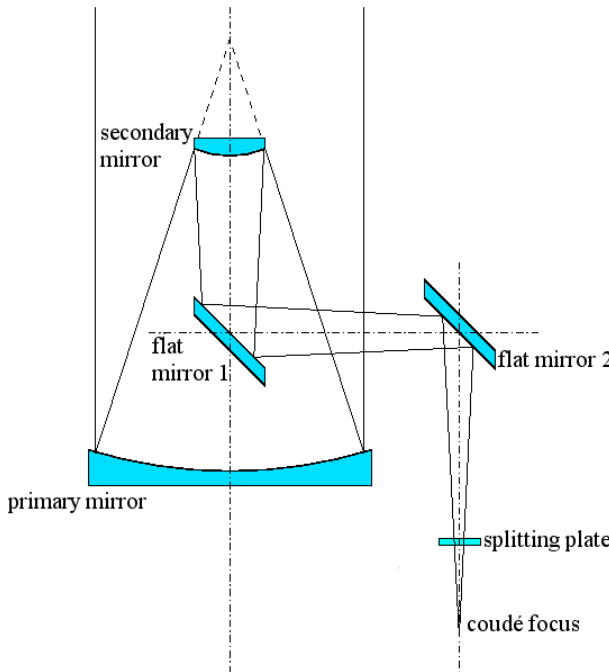


Fig. 2. Optical layout of Perek 2 m Telescope [3]

where  $d$  is distances of grooves,  $\theta_m$  is a diffraction angle at which maxima occurs,  $\lambda$  is lights wavelength and  $m$  is a integer denoting spectral order. Multiple spectral orders can result in multiple wavelength interfering with each other (see 3). As first spectral order of light with wavelength  $\lambda$ , will fall to the same spot as second order of wavelength  $\lambda/2$

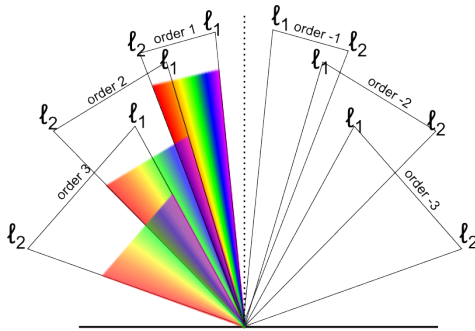


Fig. 3. Diffraction orders produced by a grating for multiple wavelengths

In order to prevent interference multiple different approaches can be used. Echelle type spectrographs use cross-dispersing element to spatially separate diffraction orders on the detector – this enables them to measure very wide spectrum in a single image. A simpler approach is to use filters to block out light of wavelength that would interfere with the observation. Or do observation in an order where possible interfering wavelength fall bellow capabilities of the CCD detector or the optical system itself. Coudé spectrograph connected to Perek telescope employs both approaches [4].

#### IV. COUDE SPECTROGRAPH

The coudé spectrograph at the Ondřejov Observatory operates as a single order spectrograph operating either in first or second order depending on what range of wavelengths is observed I. Basic components of the spectrograph are an entrance slit or fiber, a collimator, a dispersive element, a camera system and a detector, as seen on picture 4.

TABLE I  
SPATIAL FLATFIELD ANALYSIS GAIN ESTIMATES

Spectral order	$\lambda_{\min}$ (Å)	$\lambda_{\max}$ (Å)
1	5100	9100
2	3700	5100

Light that enters the spectrograph through the slit or optical fiber, collimating into a parallel beam. In this beam, the diffraction grating is encountered, which separates the light according to wavelength. Next, the dispersed light is subsequently focused onto the CCD detector by camera optics, where the spectrum is recorded. This final assembly froms a Schmidt camera with focal length of 700 mm.

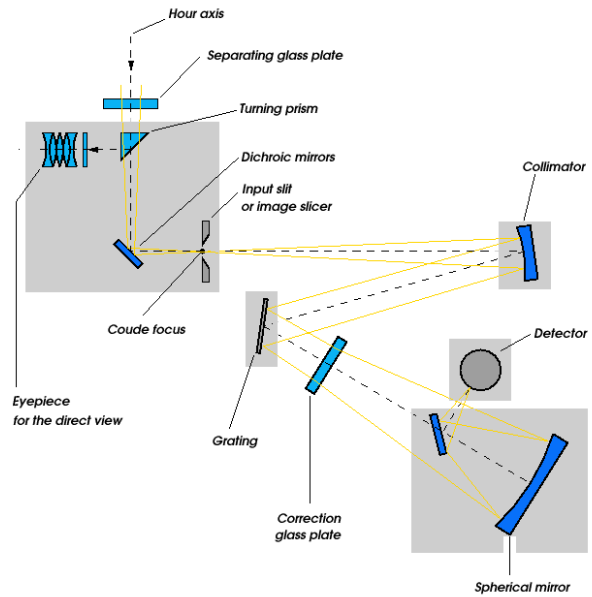


Fig. 4. Optical layout of a coudé spectrograph [3]

A PyLoN eXcelon type of CCD assembly is used with chip E2V 42-10 BX. The chip is cooled using liquid nitrogen to operating temperature of -115°C. For calibration a Thorium-Argon reference lamp is installed and driveen at 15 mA [3].

#### V. CCD DETECTOR FUNDAMENTALS

Charge-Couple Devices are widely used in astronomical spectroscopy since they are well suited for the detection of faint astronomical signals and for applications requiring precise spectroscopic and photometric measurements. This is because of their properties, which include high quantum

efficiency, linear response over a wide dynamic range and relatively low noise characteristics.

The operating mode of these devices is that incident photons interact with the silicon substrate, generating photoelectrons through the photoelectric effect. This way, the number of generated electrons is proportional to the incident photon flux and the detector quantum efficiency. The generated photoelectrons are accumulated in potential wells associated with individual pixels during the exposure time. Then, using a sequence of clocked voltage shifts, the stored charge is transferred across the detector and eventually read out at an amplifier. In this readout process, the collected charge is converted to a voltage signal in order to be digitized by analog-to-digital converter (ADC) and recorded in units of Analog-to-Digital Units (ADU). During this process, several instrumental effects that have to be characterized and corrected during data reduction are introduced [2].

The CCD gain determines the conversion between the number of electrons and the recorded ADU value, in units of electrons per ADU

$$N_{e^-} = G \cdot S_{\text{ADU}}. \quad (2)$$

Knowledge of this gain is essential for converting measured signals into physically meaningful quantities and for correctly estimating the contributions of different noise sources. Incorrect gain value can leads to systematic errors in noise estimations and subsequently in signal-to-noise ratio calculations, affecting the reliability of scientific results [1].

Another important characteristic of CCD detectors is their linear response, which assures that the recorded signal is proportional to the number of incident photons over a wide range of illumination levels. The assumption of linearity is crucial for many calibration procedures, such as flat-field correction and gain determination. Deviations from linearity may occur at very low signal levels due to electronic effects or near full-well capacity due to charge saturation. Consequently, linearity tests are commonly performed to verify the operational range of the detector [1].

In addition to gain and linearity, CCD performance is influenced by pixel-to-pixel variations in sensitivity, commonly referred to as pixel response non-uniformity. These variations arise from manufacturing imperfections and are corrected using flat-field calibration frames. Understanding the physical operation of CCD detectors and their fundamental characteristics is therefore essential for the correct interpretation of spectroscopic data and forms the basis for the calibration and noise analysis procedures described in subsequent sections.

## VI. NOISE SOURCES IN CCD DETECTORS

Several independent noise sources affect measurements performed with CCD detectors. The main contributions are read noise, dark current noise, and photon (shot) noise. A clear understanding of the physical origin and statistical properties of these noise sources is essential for interpreting CCD data and for optimizing observational strategies.

Read noise is introduced during the electronic readout process of the CCD and is independent of the exposure time. It comes from multiple electronic components, such as the output amplifier, the charge-to-voltage conversion stage or the analog-to-digital converter. Fluctuations in the process of the readout lead to uncertainty in the measured signal, even in the absence of incident light.

Read noise is typically characterized using bias (zero-exposure) frames, which record the electronic offset and readout fluctuations of the detector. By analyzing the statistical dispersion of pixel values across multiple bias frames, the read noise can be estimated on a pixel-by-pixel basis or as a global detector parameter. Read noise limits low signal levels, where it can dominate over other noise sources and significantly reduce the signal-to-noise ratio. This happens because read noise does not depend on exposure time, as the collected signal increases, its relative contribution decreases. To achieve reliable measurements, read noise has to be minimized for short exposures or observations of faint sources. Read noise should follow Gaussian (normal) distribution, as it originates from the sum of many independent electronic processes in the readout chain [2].

Dark current noise arises from thermally generated electrons within the silicon lattice of the CCD, even when no light is incident on the detector. These electrons generate because of thermal excitation and are indistinguishable from the photoelectrons that come from incident photons. As a result, dark current introduces an additional signal that accumulates linearly with exposure time.

Dark current strongly depends on detector temperature and can increase rapidly with the slightest temperature changes. To minimize this, CCD detectors are commonly cooled, avoiding the temperature changes and reducing the dark current and associated noise. In detectors that have a good cooling system, the contribution of dark current noise may become negligible compared to other noise sources. Dark current noise follows Poisson statistics, since it is generated by random thermal electron production events within the CCD lattice [5].

Lastly, the other noise source that can be found is the photon noise, sometimes referred to just as shot noise, which originates from the statistical nature of photon arrival at the detector – thus it isn't a property of the detector itself. The number of detected photons fluctuates from one exposure to another even for a constant light source, since they arrive at the CCD detector following Poisson statistics. The uncertainty these fluctuations contribute to the detected signal cannot be eliminated by calibration. If photons are detected during the exposure, the corresponding shot noise is given by:

Photon noise becomes the dominant noise source at high fluxes since it increases with signal level. Compared to read noise and dark current noise, photon noise represents a fundamental physical limit and cannot be reduced by just making instrumental improvements. The way to reduce its relative impact would be by increasing the signal level where it is stated that it can be reduced through longer exposure times or larger telescope apertures. Photon noise also follows a Poisson

distribution, reflecting the stochastic nature of photon arrival at the detector [1].

Finally, these different noise sources must be considered together. Assuming the noise sources are statistically independent, the total noise in a CCD pixel is given by the quadratic sum of all contributions:

$$\sigma_{\text{total}}^2 = \sigma_{\text{read}}^2 + \sigma_{\text{dark}}^2 + \sigma_{\text{shot}}^2. \quad (3)$$

This expression provides a practical framework for evaluating detector performance and for optimizing exposure times in spectroscopic observations [1], [2]. Understanding which noise source dominates under given observational conditions is essential for designing efficient observing strategies and for interpreting the measured data.

## VII. CALIBRATION FRAMES

Calibration frames are required in any configuration of the CCD detectors since there are instrumental effects present in CCD data. These different types of calibration frames are essential to separate the true astronomical signal from the detector and instrumental related contributions. Different contributions are needed to address different aspects of the detector response. The most used ones are bias frames, dark frames and flat-field frames.

Going into more depth of these types of calibration frames, bias or zero-exposure frames are used to measure the electronic offset introduced during the readout process and to characterize the read noise of the detector. Since bias frames are acquired with no light incident on the CCD, they contain only the electronic bias level and readout fluctuations. As stated in [2], by combining multiple bias frames, a master bias frame can be constructed and subsequently subtracted from all other images to remove this electronic offset. This is represented as:

$$I_{\text{bias-corrected}} = I_{\text{raw}} - B_{\text{master}}. \quad (4)$$

Next, dark frames are acquired with the same exposure time and detector temperature as the science observations but without any incident light. They are used to characterize the dark current and its associated noise. The accumulated dark signal increases linearly with exposure time and depends strongly on detector temperature. From [1], dark frames can also capture fixed-pattern components of the dark signal, such as hot pixels. These can be removed by subtracting a master dark frame from the data.

Finally, flat-field frames are used to correct for pixel-to-pixel sensitivity variations and large-scale illumination gradients across the detector. In perfect conditions, flat-field frames would require a uniform illumination of the CCD, but in practice, this perfect uniformity is next to impossible to achieve. In fiber-fed spectrographs, variations in fiber positioning or illumination can introduce additional gradients in the flat-field images. As stated in [1], these effects must be carefully accounted for during calibration to avoid introducing

systematic errors into the corrected spectra. They are corrected following the next equation:

$$I_{\text{flat-corrected}} = \frac{I_{\text{raw}} - B_{\text{master}} - D_{\text{master}}}{F_{\text{norm}}}, \quad F_{\text{norm}} = \frac{F_{\text{master}}}{\langle F_{\text{master}} \rangle}. \quad (5)$$

## VIII. BIAS FRAME ANALYSIS

15 bias frames were taken at lowest exposition time possible. Exact time in seconds is not known as camera limitations induce some static delay. Later on from dark frames it was estimated to be around half a second, but for the purpose of analyzing zero frames it doesn't play a role and neither was a lot of attention given to making the offset estimate particularly accurate.

Analysis of bias frames from the spectrograph is relatively straightforward. First of all median frame was created, to remove any fixed-pattern CCD might exhibit. Median is used to prevent master frame from being influenced by any high energy particles that might impact the sensor during short observation and sway the results. For master frame and stack of all bias frames basic statics were calculated as showed in table II.

TABLE II  
BIAS FRAME ANALYSIS RESULTS

Data	$\mu$ (ADU)	$\sigma$ (ADU)
Master frame	600.15	1.18
All bias frames	600.14	3.62

We can see that the readout noise is fairly small and also from really low deviation within master frame that the sensor doesn't exhibit any noticeable fixed-pattern (also apparent from 5). Below are images, one for statics calculated within master frame 6, second for all zeros taken 7. As some high energy particles impacted the sensor in some frames second histogram limited to at max 625 ADU. Still it is clearly visible that the measured noise has expected Gaussian distribution.

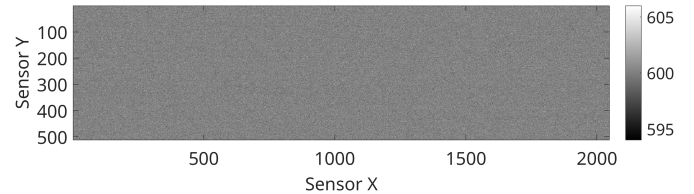


Fig. 5. Master Zero Frame

## IX. DARK FRAME ANALYSIS

All together four dark frames were taken each with one hour long exposition. At first master zero frame was subtracted from all dark frames, to remove any fixed-pattern, regardless how small. Multiple different properties were then observed. Those were dark current characteristics, number of hot pixels and transient events (which needed to be filtered out).

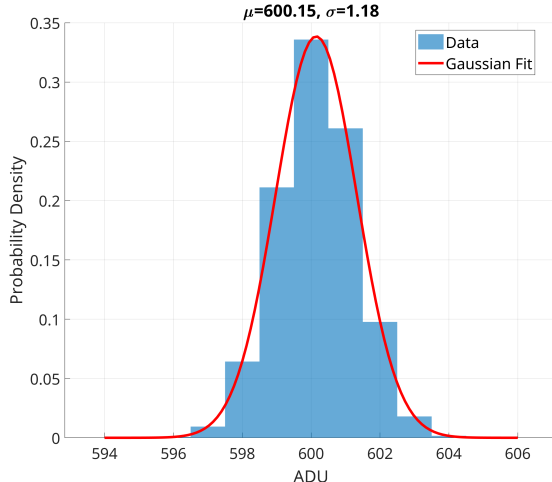


Fig. 6. Master Zero Frame Uniformity

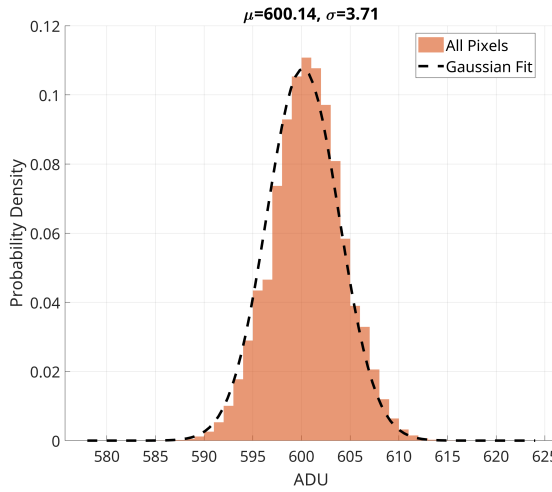


Fig. 7. Total Zero Stack Noise Distribution

A threshold for hot pixels was set to be a values higher than 5 times the standard deviation of the master dark frame, according to [6]. In individual dark frames it would be impossible to distinguish between high energy particles impacting the sensor and hot pixels thus this analysis was only run on the master dark frame, since hot pixels should exhibit values significantly higher then mean in all images. For threshold of 5 times the standard deviation 252 such pixels were found, this comprises 0.024 % of the area of the CCD sensor. If a much more conservative threshold of 10 times the standard deviation would be used only 17 pixels would have met this criteria. Thus it's also apparent that sensor exhibits quite good thermal noise uniformity.

Some of these hot pixels fall within areas that are illuminated by the light coming from the dispersive grating. However most pixels (177 or 69.4 %) are isolated and don't form any larger cluster, so their impact on measurement should be negligible. Remaining 77 have another hot pixels in their

vicinity (checked by doing 2D convolution using 5x5 matrix of ones). With largest groups having as many as 10 pixels close to each other, which could possibly be a small manufacturing defect. Their locations can be seen on picture 8, each dot has a size of 30 pixels as to be visible.

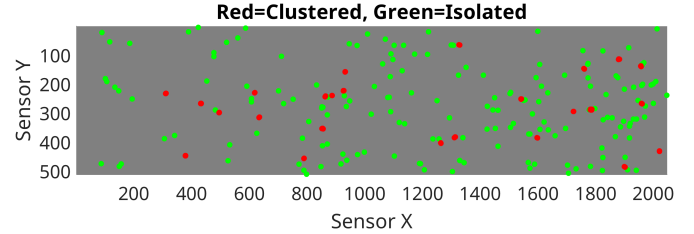


Fig. 8. Hot Pixels Locations

Aside from constantly hot pixels transient events were also detected. As already stated, while hot pixels will exhibit high values on all dark frames, pixels effected by transient event (cosmic rays, background radiation) will be hot only on single frame. Taking a maximal value for each pixel from all darks and comparing it to median dark frame, some 707 pixels were over a threshold of 1000 ADU.

As for statistical properties of the dark frames. Master dark frame exhibits a low standard deviation of 2.01 ADU, with average values of 1.89 ADU. Deviation calculated over all frames is 6.77 ADU, when transient events are excluded this drops to 6.02 ADU. Verifying if the measured data follow expected distribution is rather difficult. Shot noise from dark currents should exhibit Poisson distribution, however as it's variance is quite small – that is comparable with one for readout noise – it's difficult to accurately separate both noises. While variance of read noise and master zero is known, this noise is still present in darks and cannot be easily subtracted.

In order to express dark currents in accurate units  $e^{-} s^{-1}$  gain value of  $0.6114e^{-} \text{ADU}^{-1}$ , estimated in following chapters, was used. Using this gain mean dark current was  $0.342 \cdot 10^{-3} e^{-} s^{-1} \text{px}^{-1}$  with deviation of  $0.321 \cdot 10^{-3} e^{-} s^{-1}$ . It clearly holds that  $\mu = \sigma = \lambda$  which is to be expected for Poisson statistical distribution. Distribution of dark current overlaid with Poisson distribution curve for calculated  $\mu$  and  $\sigma$  is showed on picture 9.

## X. GAIN CALCULATION

In order to estimate gain 60 different images with different exposure times and at four different illumination intensities were taken. Light source was ambient light in the telescope dome. Different light intensities were achieved by offsetting optical fibres that bring light to the spectrograph relative to each other. Thus no prior information on how much did different intensities differ was known.

Basic idea for noise calculation stems from the fact that arriving photons exhibit a Poisson distribution. Normally for Poisson distribution mean value and variance are equal to each other. However when amplification/attenuation is present this doesn't hold true and gain value needs to be included into

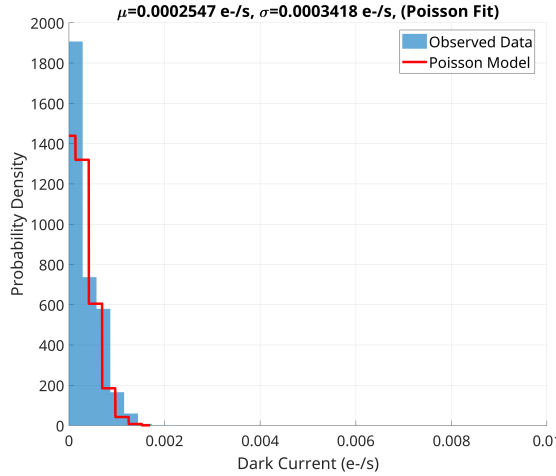


Fig. 9. Dark Current Distribution

equation. If we also add influence of other noises (here just read noise  $\sigma_{\text{ro}}^2$ ) we get an equation

$$g \cdot \sigma = \sqrt{\bar{x} \cdot g + \sigma_{\text{ro}}^2}. \quad (6)$$

As the noise is statistically independent it's simply included in the sum,  $\bar{x}$  is mean signal value,  $\sigma$  it's standard deviation and lastly  $g$  is gain [7].

This equation is often modified for the purpose of numerical calculation as

$$\sigma^2 = \frac{\bar{x}}{g} + \frac{\sigma_{\text{ro}}^2}{g^2}. \quad (7)$$

This removes unnecessary step of calculating square root.

In non where sensor installation can enable a uniform flatfields illumination good gain estimate can be made from just a couple of images [8]. Variances can also be calculated easily across different pixels - if their properties are similar. Coulde spectrograph in Ondřejov however doesn't allow an easy modification to the structure to ensure uniform illumination of the sensor. Incoming light thus still comes through the spectral dispersive grating and different parts of spectrograph are then illuminated with different light intensities and at different wavelength. As the light source doesn't have an constant spectrum illumination will thus be strictly uniform. In addition but a small part of the sensor is actually illuminated - there are two thin strips each for one of two optical fibres brining light to the sensor, while most of the sensor area is unilluminated.

#### A. Inter-Frame Flatfield Analysis

First tested approach to calculate gain was based on calculating variances and means for groups of images of a same exposure time. Variances were thus calculated not over groups of multiple pixels but for each pixel independently as guided by [9]. Images, after subtraction of master zero frame, were first group by same illumination level and exposure. Then for groups where more than one image was present statistical properties were calculated.

While for transient event detection in dark frames simple outlier rejection method based on  $\bar{x} + n \cdot \sigma$  threshold was deemed sufficient here a more robust rejection method was implemented. This was done as in individual bins there might not be that many points and standard deviation might become significantly influenced by outliers – thus not rejecting them properly. Instead a median absolute value (MAD) was used. MAD relies on median, which is much less likely to be influenced by outliers, otherwise the basic principle is similar to classical thresholding. Mean values of the data are sufficiently large for central limit theorem to apply [10]. Thus a classical MAD scaling value of 1.4826 was kept, while cutoff value was chosen empirically based on data histogram.

Problem of this approach was that dataset contains multiple images for the same configuration only for low exposure times (bellow 10 seconds). Thus only values under 6000 ADU were accounted for in the gain calculation 10. This was deemed to be insufficient as peak value of the 16 bit is more than ten times larger.

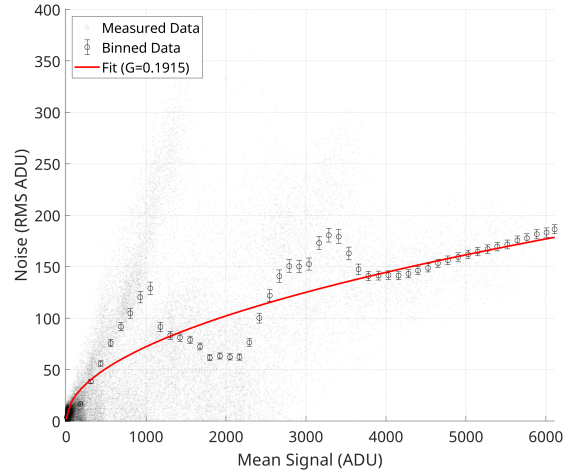


Fig. 10. Photon Transfer Curve – Inter-Frame Analysis

Gain value of  $g = 0.1915$  was calculated using this method. Due to problematic nature of this approach it's confidence intervals weren't calculated and read noise wasn't set to scale with  $\frac{1}{g^2}$ . Still it's apparent that the sensor doesn't exhibit expected behavior and thus it's gain isn't completely linear. There's especially a visible trend of median deviator values at low ADU levels increasing much faster than they should. Or it's also possible that fibre alignment wasn't as steady as it should be and spectral lines were slightly shifted between images.

#### B. Spatial Flatfield Analysis

As at least pixels properties are relatively constant in the sensor it was attempted to estimate gain while calculating statistical properties within individual pictures. In X axis are separated different wavelength it wouldn't be correct to group pixels in this direction. In Y direction however only one spectral line is present, however still not whole sensor is

illuminated by it and even within bands with spectral lines brightness level isn't constant. Still were the gain values constant across different bin sizes it would provide some useful data.

However as shown on table III gain value changes significantly with bin sizes. And even when visualizing binned data it's clear that the trend isn't there 11.

TABLE III  
SPATIAL FLATFIELD ANALYSIS GAIN ESTIMATES

Bin Height (px)	Gain ( $e^-/\text{ADU}$ )
2	0.1211
3	0.0854
4	0.0826
5	0.0401

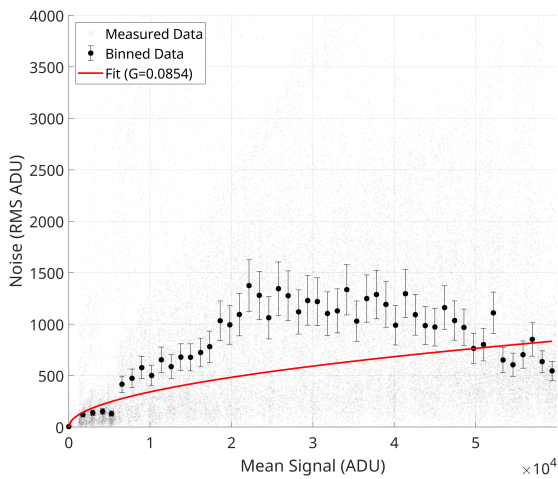


Fig. 11. Photon Transfer Curve – Spatial Analysis, Bin Size = 3

### C. Residual Flatfield Analysis

Upon mentors suggestion residual analysis method for gain estimation was attempted. Instead of calculating variance between real values, be it between two images or from bins, model is first created that is close to free from noise and variance from this model is then calculated. Data processing algorithm works in following steps: I

- 1) First images are grouped based on illumination intensity (That is by different fibre positions).
- 2) Each group is then processed separately.
  - a) Model is created from images in the group. This model is normalized to have a mean value of one.
  - b) For each image model is scaled.
  - c) Residual for each pixel is calculated.
  - d) Mean value is taken as the model value.
- 3) Stratified sampling.
- 4) Outlier rejection using MAD.
- 5) Calculate local gain in for each level.
- 6) Fit a  $\sigma^2 = \bar{x} + \frac{\sigma_{ro}^2}{g^2}$ .

Main problem of this method is the creation of accurate model, that is free of noise. This model is created by calculating a mean value for each pixel over set of images.

One approach was to use largest set of images of the same exposure. In the processed dataset this occurst for the 10 second exposition time, for illumination level with the most data. Some illumination levels don't have pairs of images at all, so averaging accross single exposure time cannot be done. Regardless when averaging same images we should see reduction of

$$\sigma_N = \frac{\sigma}{\sqrt{N}} \quad (8)$$

where  $\sigma_N$  is noise deviation after averaging and  $N$  is the number of averaged images [10]. At 9 frames we have a noise reduction of just 67 %.

As this model is created for rather low ADU leves (at most around 6000), when scaled up remaining noise causes significant error. On image 12 is the photon transfer curve when such a model is used. It's apparent that the model work really well for low values – where the points follow the square root dependence rather well, however for larger values model breaks down as the remaining noise get's significant amplified in the scaling. Models failure can also be demonstrated best on residual histograms (images 13 and 14), where not only shape of the curve itself is wrong but also mean estimate isn't clearly correct.

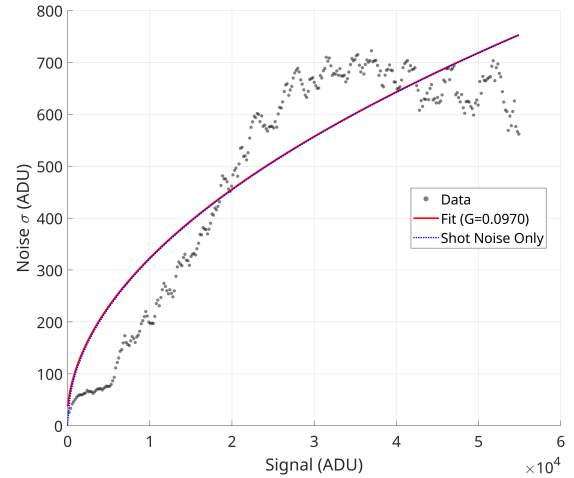


Fig. 12. Photon Transfer Curve – Residual Analysis, 10 s Exposure Model

It was also attempted to filter out the model as a 1D signal (going from top to bottom across the 512 px, and left to right). Since in horizontal direction changes in illumination should be quite smooth as we aren't going across different spectral lines and previous sections shown that deviations between pixels are small. However this approach didn't significantly improve the calculation.

Due to the failure of the model based on most numerous exposure time an model based on mean of all flatfields was used. This model tackles higher values much better although still is far from perfect as due to datasets nature there are

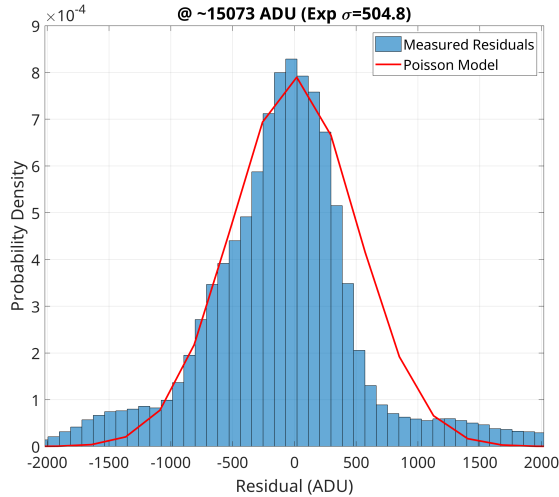


Fig. 13. Residual Histogram at Median, 10 s Exposure Model

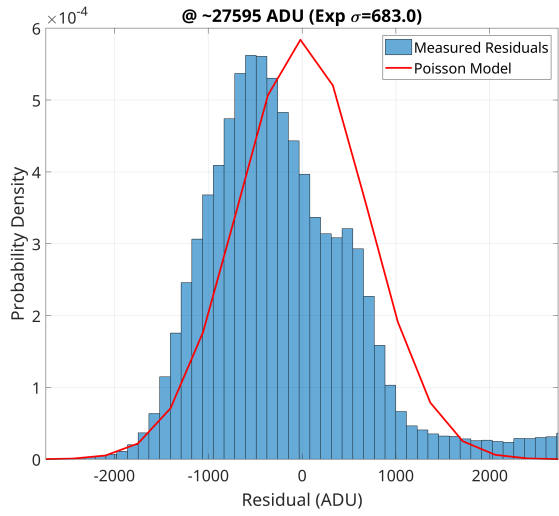


Fig. 14. Residual Histogram at 3rd Quantile, 10 s Exposure Model

significantly less images for higher exposure times. So their noise contribution will be less suppressed and as their values are much higher they will sway the model estimate their way.

Another step in processing is scaling the model to each flatfield level. This isn't particularly complicated as flatfields energy raises rather linearly with exposure time as seen on picture 15. Only minor departure from the straightforward approach was to filter out pixels that aren't illuminated when finding the scaling coefficient - as those would drag down the model and lead to bad mean estimates. In the model itself these inilluminated parts are also zeroed so that after scaling them the values don't rise, same way they don't rise in the real flatfields for longer exposures.

After model is scaled residual from it are calculated and stored. In following step stratified sampling is applied to the points – this lowers data count from some  $\approx 12$  million to 2 and doesn't introduce any measurable error. This sampling

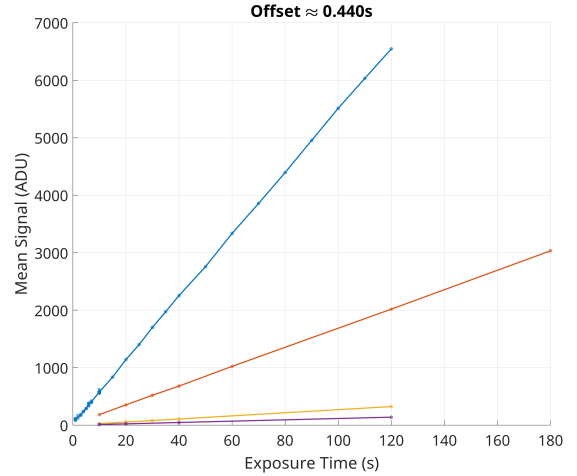


Fig. 15. Flatfield Levels vs Exposure Time, Different Illuminations

just splits measured data into bins according to their signal level and in each bin takes a random subset of point. Stratified sampling is necessary as the distribution of data points between bins is far from uniform.

Following startified sampling outlier rejection using MAD is applied. Then in the cleaned data equation 7 is fitten in and the gain is calculated, while read noise is fixed to the value calculated from zero frame analysis.

A gain value of  $g = 0.6114 \pm 0.0045 \text{ e}^{-}\text{ADU}^{-1}$  was estimated using this method. This gives a following photon transfer curve 16.

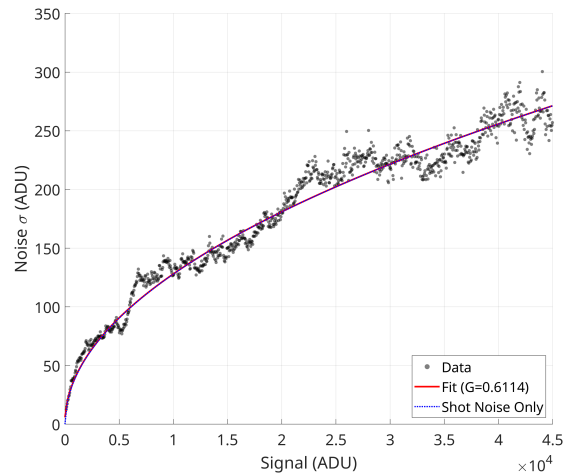


Fig. 16. Photon Transfer Curve – Residual Analysis

Still it must be said that the dataset is fundamentally flawed and much denser dataset with more uniform distribution of exposure times might give different results. Plot 17 shows the gain value calculated for each signal level individually. A simpler equation of  $\sigma^2 = \bar{x}/g + \sigma_{ro}^2$  was used combined with low number of data in each bin straight line cannot be even expected, but it's clear that the gain estimation is still problematic. This is despite overall good confidence interval

the model when overlaying the function across all data. For this reason a gain linearity (gain as a function of intensity) wasn't explored at all.

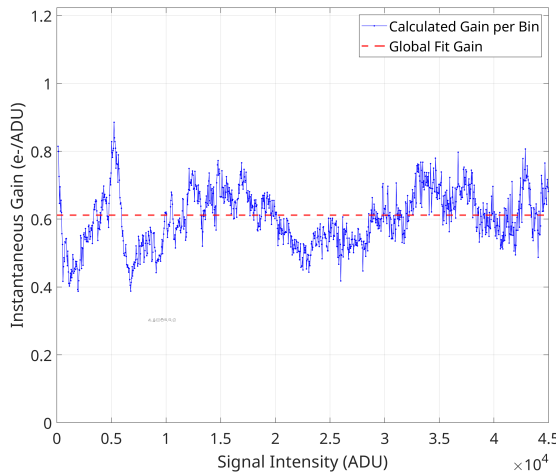


Fig. 17. Model Local Gain

## XI. GRATING POSITION AND SENSOR RESOLUTION

Last examined parameter of the Coudé spectrograph was to verify if documentation (see [3]) on relation between central wavelength on grating orientation and resolution of the spectrograph was correct. For this purpose reference spectra of ThAr lamp were taken and compared against atlas of strong spectral lines of Thorium [11] and Argon [12]. Automating this task proved to be rather complex – for each frame resolution ( $\text{\AA} \text{px}^{-1}$ ) and central wavelength ( $\text{\AA}$ ). If close to linear relationship between grating angle and central wavelength is to be expected than three variables must hold for each image – slope ( $\text{\AA} \text{rad}^{-1}$ ), intercept point ( $\text{\AA}$ ) and resolution ( $\text{\AA} \text{px}^{-1}$ ).

Method based on geometric hashing was employed where first triples of peak were found within measured data and then atlas was searched for peak with same relative distances. For matches atlas was then scaled and offset (Also convolution with Gaussian function was applied to "spread" the lines a little bit.) and relative energy was calculated based on which parameter estimated was scored. However as some spectral lines weren't emitted from the 15 mA ThAr lamp at all and some spectral lines that were captured weren't in the atlas this method failed to find correct match.

Lines were then matched manually on selected few pictures and output parameters. Those were found to generally correspond with those listed in the documentation – tables V and ??

## XII. CONCLUSION

Coudé spectrograph on Perek 2 m telescope exhibits quite good noise parameters and pixels are generally uniform. Read noise was measured at 3.62 ADU, and found to follow Gaussian distribution without any anomalies across sensor area. Mean dark current was  $0.342 \cdot 10^{-3} \text{ e}^{-\text{s}^{-1}\text{px}^{-1}}$  with

TABLE IV  
THE RANGES OF EXPOSED SPECTRA – FIRST ORDER [3]

Grating Increment	Grating Angle (deg)	Min ( $\text{\AA}$ )	Max ( $\text{\AA}$ )
5321	35.78	8401.4	8869.9
5430	35.25	8197.2	8666.3
6382	30.62	6406.2	6878.6
6457	30.25	6263.5	6736.0
6943	27.88	5328.6	5801.4

TABLE V  
THE RANGES OF EXPOSED SPECTRA – SECOND ORDER [3]

Grating Increment	Grating Angle (deg)	Min ( $\text{\AA}$ )	Max ( $\text{\AA}$ )
4712	38.75	4758.8	4991.1
5040	37.15	4459.9	4693.4
5242	36.17	4273.7	4507.7

deviation of  $0.321 \cdot 10^{-3} \text{ e}^{-\text{s}^{-1}}$ , thus it shouldn't pose a major problem in long exposure imaging even of relatively faint objects. Sensor also exhibited only a small number of hot pixels.

Gain calculation proved to be problematic due to nature of the dataset used. Simple inter-frame methods didn't yield good results as only about tenth of the CCD range was covered by them. Intra-frame methods couldn't work due to nature of spectostrophic images where flatfields illumination is unequal. Lastly attempted was a residual method that estimated the gain at  $g = 0.6114 \pm 0.0045 \text{ e}^{-\text{ADU}^{-1}}$ . However the model used in it was far from perfect and even with low uncertainty error of this method might be significant.

## ACKNOWLEDGMENT

The authors would like to thank the Astronomical Institute of the Czech Academy of Sciences for providing access to the Ondřejov Observatory facilities and for their support during the measurements.

## REFERENCES

- [1] P. Martinez and A. Klotz. *A Practical Guide to CCD Astronomy*. Cambridge University Press, 2001.
- [2] S. Moore and R. Gendler. *Lessons from the Masters: Current Concepts in Astronomical Imaging*. Springer, 2014.
- [3] Miroslav Šlechta. Ondřejov perek 2-m telescope – overview, 2024.
- [4] Miroslav Šlechta. Coude spektrograf, 2024.
- [5] Thomas Fellers and Michael Davidson. Ccd noise sources and signal-to-noise ratio.
- [6] Louisa Kennedy and Peter Young. Hinode EUV imaging spectrometer (EIS) software note no. 6: Warm and hot pixels on the EIS CCDs. Technical report, Mullard Space Science Laboratory, University College London and NASA Goddard Space Flight Center, feb 2020.
- [7] Michael Newberry. Ccd camera gain measurement, 1996.
- [8] Iraf documentation, findgain function.
- [9] J. Gordon Robertson. Spectroscopic flat-fields can be used for precision ccd gain and noise tests. *Publications of the Astronomical Society of Australia*, 38:e006, 2021.
- [10] Ronald E. Walpole, Ye Keying, Raymond H. Myers, and Sharon L. Myers. *Probability & statistics for engineers & scientists*. Prentice-Hall, Upper Saddle River, NJ, 7th ed edition, c2002.
- [11] A. Palmer and R. Jr. Engleman. *Los Alamos Natl. Lab. Report LA-9615*. 1952.

- [12] Göran Norlén. Wavelengths and energy levels of ar i and ar ii based on new interferometric measurements in the region 3 400-9 800 Å. *Physica Scripta*, 8(6):249–268.